Protein-flexibility mediated coupling between photoswitching kinetics and surrounding viscosity of a photochromic fluorescent protein

Ya-Ting Kao[1], Xinxin Zhu[1], and Wei Min[2]

Department of Chemistry, Columbia University, New York, NY 10027

Edited by Robin M. Hochstrasser, University of Pennsylvania, Philadelphia, PA, and approved December 27, 2011 (received for review September 19, 2011)

Recent advances in fluorescent proteins (FPs) have generated a remarkable family of optical highlighters with special light responses. Among them, Dronpa exhibits a unique capability of reversible light-regulated on-off switching. However, the environmental dependence of this photochromism is largely unexplored. Herein we report that the photoswitching kinetics of the chromophore inside Dronpa is actually slowed down by increasing medium viscosity outside Dronpa. This finding is a special example of an FP where the environment can exert a hydrodynamic effect on the internal chromophore. We attribute this effect to protein-flexibility mediated coupling where the chromophore's *cis-trans* isomerization during photoswitching is accompanied by conformational motion of a part of the protein β-barrel whose dynamics should be hindered by medium friction. Consistent with this mechanism, the photoswitching kinetics of Dronpa-3, a structurally more flexible mutant, is found to exhibit a more pronounced viscosity dependence. Furthermore, we mapped out spatial distributions of microviscosity in live cells experienced by a histone protein using the photoswitching kinetics of Dronpa-3 fusion as a contrast mechanism. This unique reporter should provide protein-specific information about the crowded intracellular environments by offering a genetically encoded microviscosity probe, which did not exist with normal FPs before.

protein conformation flexibility | photoisomerization

Green fluorescent protein (GFP), first isolated from the bioluminescent *Aequorea victoria* jellyfish, and its variants are widely used as genetically encoded reporters in bioimaging applications (1–4). These fluorescent proteins (FPs) fold into a rigid 11-stranded β-barrel with a coaxial central helix holding an autocatalytically derived chromophore and short helical segments capping both ends of the barrel (5). As a consequence, the GFP chromophore, Ser^{65}-Tyr^{66}-Gly^{67} (SYG), is encapsulated within the protein matrix and well-shielded from the bulk solvent. Hence, unlike organic fluorophores whose fluorescence lifetimes are often sensitive to solvent viscosity, the medium viscosity surrounding the FPs has no correlative effect on the fluorescence intensity or lifetime of GFP variants (6–8). To our knowledge, there are no previous reports on GFP-based viscosity sensors.

Recently, several distinct classes of FPs, such as photoactivatable, photoconvertible, and photoswitchable FPs, have drawn considerable interest, owing to their special light responses. The chromophores of these FPs can either be activated to initiate fluorescence from a dark state or optically converted from one color to another (9–12). Both photoactivation and photoconversion processes are irreversible. In contrast, the unique class of photoswitchable FPs can undergo reversible conversions between a fluorescent bright state and a nonfluorescent dark state upon light irradiation with appropriate wavelengths (13–15).

Among all photoswitchable FPs, Dronpa is the most studied prototype (13). As a monomeric protein, Dronpa exhibits a typical GFP-like barrel structure (Fig. 1*A*) with its chromophore, Cys^{62}-Tyr^{63}-Gly^{64} (CYG), held in the center. Notably, CYG in Dronpa adapts distinct *cis* and *trans* conformations in the bright and dark states, respectively (16–19). As shown in Fig. 1*A*, irradiating Dronpa at 488 nm generates fluorescence emission in the green channel. Meanwhile, 488-nm light can convert Dronpa to a nonfluorescent dark state with a bright-to-dark switching efficiency (Φ_{BD}) of 3.2×10^{-4}. In addition, the dark state that is formed can be efficiently converted back to the original bright state by a brief irradiation at 405 nm ($\Phi_{DB} = 0.37$) (13). The primary mechanism for Dronpa photoswitching is thought to arise from the changes in the protonation-deprotonation states and/or *cis-trans* conformations of the chromophore accompanied by regulation of structural flexibility of the protein matrix (Fig. 1*B*) (14, 17, 19). In line with these insights, several Dronpa mutants with higher structural flexibility, such as Dronpa-2, Dronpa-3, rsFastlime, bsDronpa, and Padron, are found to exhibit higher photoswitching efficiency (18, 20–22). Although the photochromism of Dronpa has been harnessed to study protein trafficking inside cells (13, 23) and to superresolution fluorescence imaging (21, 24, 25), its environmental dependence is largely unexplored.

We first report our finding that the bright-to-dark photoswitching kinetics of the original Dronpa and its Dronpa-3 mutant is actually not an intrinsic property of the internal chromophore; instead, the kinetics slows down significantly with increasing viscosity of the solvent that the protein is exposed to. To our knowledge, this finding is a unique report of the viscosity effect on the photophysics of FPs. Protein-flexibility mediated coupling between the chromophore's *cis-trans* conformational motion inside the protein and the environmental friction outside the protein is proposed as the underlying mechanism. We further demonstrated microviscosity imaging in the nucleus of live cells using the photoswitching kinetics of H2B-Dronpa-3 fusion protein as a contrast mechanism. This fusion protein would be a unique genetically encoded microviscosity reporter, which does not exist with normal FPs, enabling the characterization of the crowded intracellular local environments experienced by specific proteins of interest.

Results and Discussion

Photoswitching Trajectory of Dronpa Under the Microscope. Our modified confocal setup is shown in Fig. 2. In particular, we control both the beam size and temporal switching of two excitation beams (For more details see *Materials and Methods*). Fig. 3*A* shows a typical fluorescence intensity trajectory of Dronpa in aqueous buffer. When the 405-nm light is switched on at the same time as the 488-nm light, the bright green fluorescence appears immediately because of efficient photoswitching from the dark state to the bight state by the 405-nm light. When the 405-nm

Author contributions: W.M. designed research; Y.-T.K. and X.Z. performed research; Y.-T.K. and X.Z. analyzed data; and Y.-T.K. and W.M. wrote the paper.

The authors declare no conflict of interest.

This article is a PNAS Direct Submission.

[1]Y.-T.K. and X.Z. contributed equally to this work.

[2]To whom correspondence should be addressed. E-mail: wm2256@columbia.edu.

This article contains supporting information online at www.pnas.org/lookup/suppl/doi:10.1073/pnas.1115311109/-/DCSupplemental.

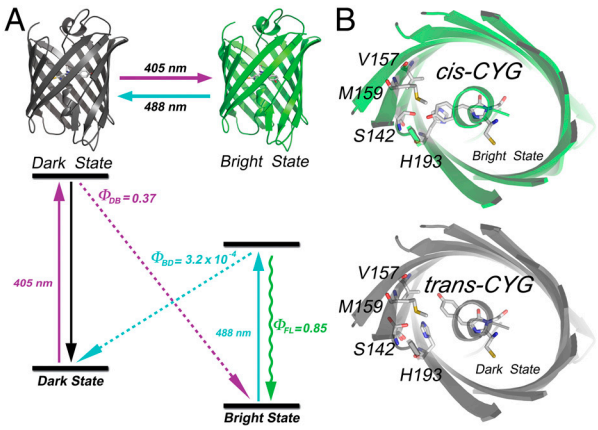

Fig. 1. Structural and photophysical characteristics of Dronpa. (*A*) Photoswitching scheme of the Dronpa protein. Upon irradiation at 405 and 488 nm, Dronpa switches between dark and bright states. Structures of the dark and bright state are shown in gray [Protein Data Bank (PDB) ID code 2POX] and green (PDB ID code 2IOV), respectively (17, 18). (*B*) Representative views of the chromophore and its nearby residues. The CYG chromophore in Dronpa adapts distinct *cis* and *trans* conformations in the bright (*Upper*) and dark state (*Lower*), respectively.

light is switched off after a 1-ms pulse duration and only the 488-nm light is illuminating the sample, the fluorescence intensity of Dronpa starts to decrease because the continuous bright-to-dark switching effect by the 488-nm light leads to dark-state build-up and concurrent bright-state population decay.

We now examine the temporal decay shown in Fig. 3*A*. With a much larger illumination area of the 405-nm beam creating a wide reservoir of Dronpa in the bright state, immediately after the 405-nm light is switched off, Dronpa molecules that are inside and outside the 488-nm confocal spot are all in the bright state,

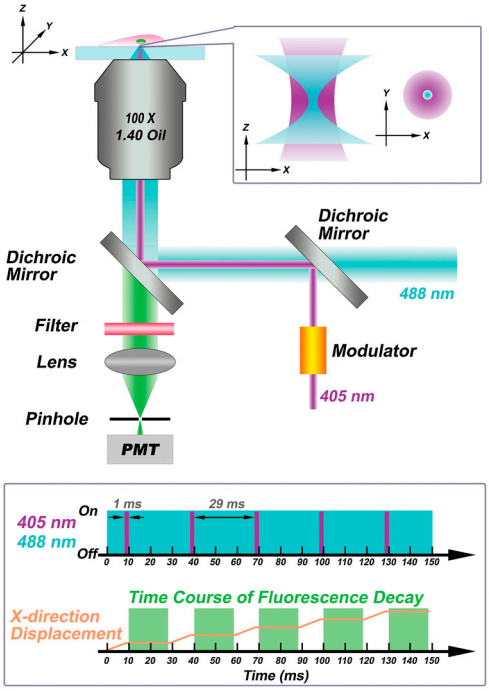

Fig. 2. Schematic of the modified confocal fluorescence microscope and illumination scheme. The 488-nm laser provides continuous illumination and it is tightly focused, whereas the pulsed 405-nm lasers, which has a smaller beam size, is loosely focused by the same microscope objective (*Upper* box). After the piezo stage moves to a new pixel every 30 ms, the 405-nm laser is switched on for only 1 ms and the time course of fluorescence emission is continuously recorded under 488-nm excitation (*Lower* box).

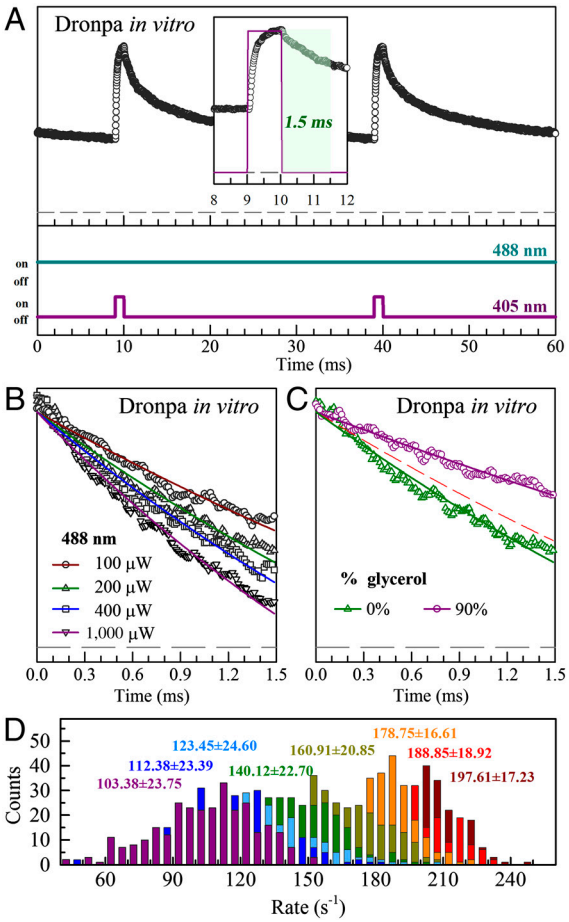

Fig. 3. Viscosity dependence of the photoswitching kinetics of Dronpa. (*A*) Fluorescence time course of Dronpa in aqueous buffer under the corresponding on-off illumination scheme of the 488-nm and 405-nm light. *Inset* shows the zoomed-in view and highlights the initial 1.5-ms duration of the fluorescence decay. The gray dashed line indicates the background fluorescence level. (*B*) Normalized initial 1.5-ms fluorescence trajectories obtained under four different 488-nm laser powers in aqueous buffer. Note that the gray dashed line indicates a normalized fluorescence intensity of 0.60. (*C*) Normalized initial 1.5-ms fluorescence trajectories of Dronpa obtained in buffer with 0 and 90% glycerol under 488-nm irradiation at 200 μW. Note that the red dashed line indicates fluorescence decay with a rate of 164 s^{-1} which is 20% slower than 197 s^{-1} and the gray dashed line indicates a normalized fluorescence intensity of 0.60. (*D*) Histograms of the decay rate obtained in buffer with different percentages of glycerol under 488-nm irradiation at 200 μW (0% dark red; 10% red; 20% orange; 40% dark yellow; 60% green; 70% pale blue; 80% blue; and 90% purple).

and hence their diffusional exchange would not affect the optical signal. However, when the 405-nm laser is turned off, more dark-state population builds up inside the 488-nm confocal spot over time, at which the diffusional exchange with the bright-state molecules in the reservoir effectively attenuates the fluorescence intensity decay. Eventually, a steady-state plateau would be reached as the result of a balance between the dark-state population generated inside the 488-nm confocal spot and the diffusion of bright-state population from the reservoir. Hence, while the steady-state plateau is convolved with diffusion dynamics of the protein molecule, the initial decay (right after the 405-nm light is off) is free from the protein diffusion contribution.

Thus, we utilize only the initial 1.5-ms fluorescence decay signal to obtain the diffusion-free photoswitching rate, as highlighted with the green color in Fig. 3*A*, *Inset*. Indeed, the initial 1.5-ms fluorescence trace can be well-fit with a single exponential decay, which implies the absence of other kinetic contributions. Moreover, we verified that the protein diffusion is insignificant at

such a short timescale based on the known diffusion constant of GFP in aqueous solution (26). As expected, the photoswitching rate constant is directly related to the illumination intensity. With higher 488-nm excitation power, more molecules were excited per unit time and faster fluorescence decay rates were observed (Fig. 3*B*).

Viscosity Dependence of Photoswitching Kinetics of Dronpa. We set out to test the viscosity effect on the switching rate by varying the glycerol percentage of solvent. As shown in Fig. 3*C*, we observed a slower apparent fluorescence decay rate when Dronpa was immersed in a buffer with a higher percentage of glycerol. Upon 488-nm irradiation at 200 μW, the fluorescence trajectories of Dronpa in solution with 0 and 90% glycerol exhibit a single exponential decay rate of 197.61 and 103.38 s^{-1}, respectively. In Fig. 3*D*, a series of detailed statistical histograms of the decay rates are shown by compiling over 300 fluorescence trajectories. With increasing solvent viscosity, a decrease in the apparent fluorescence decay rate is clearly observed. Furthermore, we performed parallel experiments under different 488-nm excitation powers. Quantitatively similar results are seen, and the average deceleration factor is about 1.97 between 0 and 90% glycerol (Table S1).

We attribute the observed deceleration factor of 1.97 of the apparent fluorescence decay rate to the viscosity dependence of the photoswitching rate, k_{BD}, based on the following analysis. Upon 488-nm excitation, the excited state of the bright-state Dronpa could undergo three competing processes: a radiative fluorescence pathway ($k_{radiative}$), a nonradiative relaxation process ($k_{nonradiative}$), or the nonradiative bright-to-dark conversion (k_{BD}). In principle, alterations in the dynamics of any of these three pathways could lead to changes in the apparent photoswitching yield, Φ_{BD}, (hence apparent fluorescence decay rate) as:

$$\Phi_{BD} = \frac{k_{BD}}{k_{radiative} + k_{nonradiative} + k_{BD}}. \quad [1]$$

As reported earlier (6, 7), the fluorescence lifetime of GFP variants is reciprocally proportional to the square of the refractive index. Assuming Dronpa also follows such a correlation, we estimate the fluorescence lifetime of Dronpa in solution with 90% glycerol (refractive index 1.458) to be 3.0 ns based on the fluorescence lifetime of 3.6 ns reported earlier for Dronpa in aqueous solution (refractive index 1.333) (27). Everything else being the same in both solutions, the decrease in Φ_{BD} due to the increase of $k_{radiative}$ cannot be more than 20% (Fig. 3*C*). Thus, the refractive-index-dependent $k_{radiactive}$ alone could not explain our observed factor of 1.97. On the other hand, one might expect a decrease in $k_{nonradiactive}$, as the protein matrix fluctuation could get constrained by the high solvent viscosity. However, according to Eq. **1**, a decrease in $k_{nonradiative}$ could only result in a higher Φ_{BD}. Therefore, the observed deceleration factor of 1.97 of the apparent fluorescence decay rate could only result from a decrease in the bright-to-dark photoswitching rate k_{BD}.

Molecular Mechanism of Viscosity-Dependent Photoswitching Kinetics. As for the underlying mechanism, we reason that the *cis-trans* isomerization of the chromophore inside Dronpa during photoswitching requires moderate translational motion of a part of the protein β-barrel whose conformational dynamics should be hindered by the frictional force exerted by viscous medium. As discussed below, our proposal is supported by previous studies carried out by NMR, X-ray crystal structure and molecular dynamics (MD) simulation approaches (14, 17, 19, 28).

In a recent NMR study, it has been demonstrated that the change in protein matrix flexibility is implicated upon bright-to-dark photoswitching of Dronpa (19). Because the photoswitching between two states involves a regulation in structural flexibility, applying a constraint on the dynamics of Dronpa protein matrix by the medium friction, in our opinion, should be able to slow down the photoswitching kinetics. Besides, crystal structural studies reveal that a cascade of structural rearrangements occur within the protein core upon bright-to-dark photoswitching (14, 17). In particular, the chromophore would have to change from the *cis*- to the *trans*- configuration and up to five nearby residues on the protein β-barrel would need to translate outward by approximately 1 Å to be able to accommodate for the spatial rearrangement of the chromophore isomerization. Hence, these observations are consistent with our picture of protein coupled chromophore isomerization (i.e., photoswitching). Moreover, the MD simulations suggest the flexibility of the chromophore and its immediate protein environment is the key to nonradiative decay process of dark-state Dronpa (28). As shown in Fig. 1*B*, the dark state of Dronpa loses both the hydrogen bond with Ser-142 and the aromatic stacking with His-193 (17, 18). Such structural changes increase the flexibility of both the chromophore and a part of the β-barrel, favoring nonradiative relaxation processes and leading to a short dark-state fluorescence lifetime of 14 ps (27). This result again implies the possibility of that regulating protein flexibility by local environments affects the accompanying process of bright-to-dark chromophores switching.

As a control experiment, we observed almost no change in the photoswitching kinetics of Dronpa in agarose gels of different percentages (Fig. S1). This result is because the above-mentioned conformation constraints on proteins is missing in the agarose gel's microchambers (29) in which proteins can still rotate and breath freely as if they are in aqueous solvent. Hence, our proposed mechanism is that light-induced mechanical motions of the *cis-trans* isomerization of chromophore inside the protein would be coupled to the medium outside the protein through the conformational flexibility of Dronpa protein.

More Pronounced Viscosity Dependence of a Dronpa Mutant. Dronpa mutants such as Dronpa-2 and Dronpa-3 have been shown to exhibit higher photoswitching efficiencies than the original Dronpa (20). Meanwhile, both mutants show multiexponential fluorescence lifetime decays and lower fluorescence quantum yields (21). The multiexponential decay kinetics in GFP variants has been associated to the higher flexibility of the chromophore in the protein environment (30, 31). The lower fluorescence quantum yield of Dronpa-2 ($\Phi_{FL} = 0.28$) and Dronpa-3 ($\Phi_{FL} = 0.33$) (21) indicates a dominant nonradiative process normally mediated by higher protein flexibility and more structural fluctuation (28). Intrigued by the higher photoswitching efficiency and the more flexible chromophore/protein conformation, we further examined the photoswitching kinetics of Dronpa-3 in various solvent compositions.

Fig. 4*A* shows a fluorescence intensity trajectory of Dronpa-3 in aqueous solution, which indeed decays faster than that of the original Dronpa (Fig. 3*A*), and it reaches to a lower steady-state plateau. Upon 488-nm irradiation at 200 μW, the fluorescence trajectories of Dronpa-3 in solution with 0 and 90% glycerol exhibit a single-exponential decay rate of 656.14 and 167.24 s^{-1}, respectively, with a deceleration factor of 3.92 (Fig. 4 *B* and *C*). Experiments under different 488-nm excitation powers were also performed and the average deceleration factor is found to be about 3.87 between 0 and 90% glycerol (Table S2). Compared to the corresponding factor of 1.97 in Dronpa, a factor of 3.87 for Dronpa-3 clearly demonstrates a more pronounced dependence on the medium viscosity (Fig. 5*A*).

We then compare the protein structures of Dronpa and Dronpa-3 in Fig. 5*B*. Note that the structure of Dronpa-3 is generated by a PyMOL maturation wizard with a double mutation (V157I/M159A). Isoleucine is more bulky than valine, thus it is in a close distance of 2.5 Å to serine142. Because the distance of 2.5 Å is shorter than the sum of the van der Waals radii of $C\delta$ in isoleucine

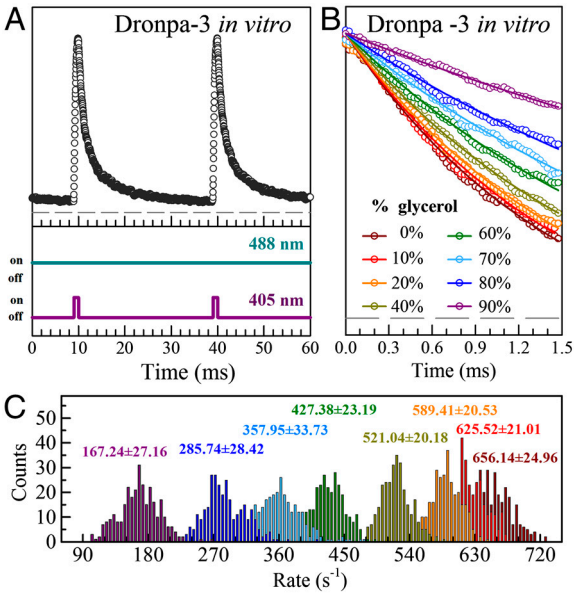

Fig. 4. Viscosity dependence of the photoswitching kinetics of Dronpa-3. (*A*) Fluorescence time course of Dronpa-3 in aqueous buffer under the corresponding on-off illumination scheme of the 488- and 405-nm light. The gray dashed line indicates the fluorescence background level. (*B*) Normalized initial 1.5-ms fluorescence trajectories of Dronpa-3 obtained in buffers with different percentages of glycerol under 488-nm irradiation at 200 μW. Note that the gray dashed line indicates a normalized fluorescence intensity of 0.15. (*C*) Histograms of the decay rate obtained in buffer with different percentages of glycerol under 488-nm irradiation at 200 μW (0% dark red; 10% red; 20% orange; 40% dark yellow; 60% green; 70% pale blue; 80% blue; and 90% purple).

and Cβ in serine, certain conformational rearrangements should occur, contributing to weakening the hydrogen bond between serine142 and the chromophore. In addition, alanine is much smaller than methionine leaving a spacious cavity to easily accommodate the dark-state chromophore. Therefore, consistent with our proposed mechanism, the higher flexibility of Dronpa-3 ultimately contributes to the photoswitching kinetics that is more sensitive to the exposed medium friction.

Furthermore, we might gain some insights about photoswitching behavior in general by lapping structures of the dark-state Dronpa and GFP together (Fig. 5*C*). It can be seen that the phenylalanine165 in GFP spatially overlaps with the dark-state Dronpa chromophore. Such a steric hindrance from protein β-barrel would severely obstruct the *cis-trans* isomerization of SYG chromophore of GFP, which might explain why the normal GFP cannot be photoswitchable. Therefore, the Dronpa family possibly owes its photoswitching capability to the remarkable flexibility of the chromophore cavity and (a part of) protein β-barrel that exerts less steric/electrostatic hindrance to the chromophore isomerization.

Genetically Encoded Microviscosity Reporter in Live Cells. Based on the discovered unique optical property of Dronpa-3, we then demonstrated its utility as a genetically encoded microenvironment probe, which has not been previously reported. As discussed earlier, the normal GFP family cannot achieve this goal because its chromophore is well-shielded from the surrounding environment by the protein matrix and consequently its fluorescence intensity and lifetime becomes unrelated to the medium viscosity (6, 7).

In our demonstration, Dronpa-3 was introduced into human embryonic kidney cells (HEK 293T) either alone or in fusion with histone H2B protein. As in in vitro assays, each scanning confocal pixel spends 30-ms duration during which the 405-nm light is on for the initial 1-ms whereas the 488-nm light is left on continuously. The regular intensity-based contrast is obtained by averaging the fluorescence intensity over 5 ms right after the 405-nm light is turned off. The photoswitching rate-based image contrast is generated by fitting the fluorescence decay of the initial 1.5-ms.

As shown in Fig. 6, all in vivo decay-rate histograms exhibit a wider distribution and a slower average rate compared to that obtained from in vitro experiments under 0% glycerol. The slower rate indicates a higher intracellular viscosity and/or crowded environments that are affecting Dronpa-3′s protein matrix flexibility. We note that although GFP in the cytoplasm shows a certain distribution in its $k_{\text{radiative}}$ due to intracellular variation of the refractive index (32), the distributions of the decay rate observed here are much wider than what could result from refractive index variation alone. Thus, our in vivo decay-rate histograms unambiguously demonstrate a more heterogeneous environment in cells.

When Dronpa-3 was expressed alone in HEK 293T cells, we obtained information about microscopic environments of the cytoplasm that are not available from regular intensity based images. As shown in Fig. 6*B*, the average decay rate observed from the cytoplasm corresponds with those observed from 20 and 40% glycerol buffers. Hence, the viscosity of the cytoplasm can be esti-

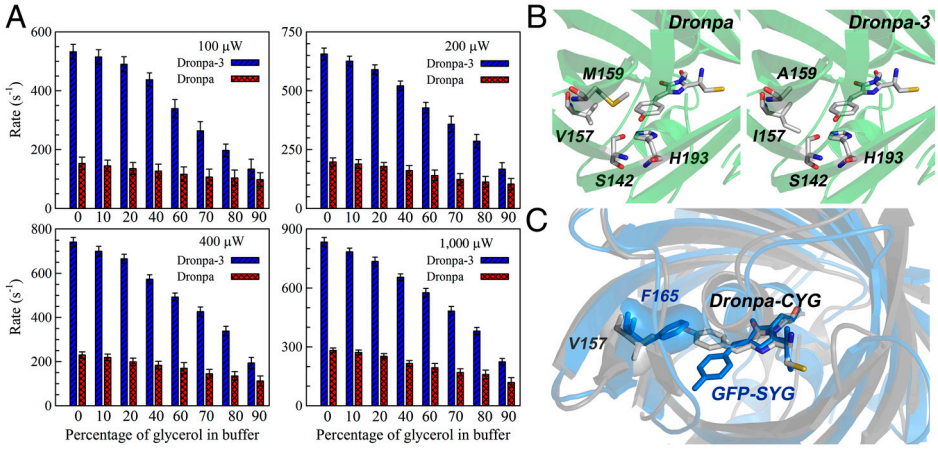

Fig. 5. Comparison between Dronpa and Dronpa-3. (*A*) The decay rate of Dronpa and Dronpa-3 under four different 488-nm laser powers and in buffer with eight different glycerol percentages. Clearly, the photoswitching kinetics of Dronpa-3 exhibits a more pronounced dependence on the local viscosity. (*B*) Structure comparison of bright-state Dronpa (18) and Dronpa-3. The Dronpa-3 structure with a double mutation (V157I and M159A) is generated by the PyMOL maturation wizard. Note that I157 (right) is in closer proximity to serine142 than V157 (left) and A159 (right) is further away from the chromophore than M159 (left). (*C*) Structural overlap of dark-state Dronpa (gray) and GFP (blue) (5, 17). The protein surface of F165 in GFP is shown in blue. Note that protein surface of F165 is overlapping with the CYG chromophore.

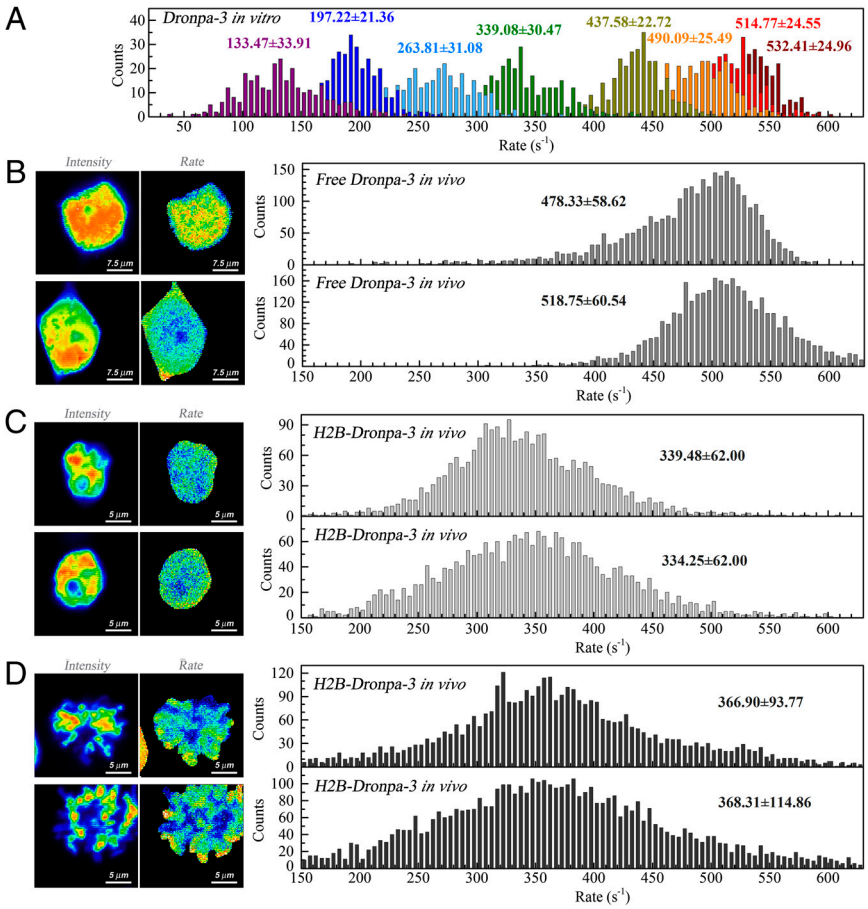

Fig. 6. Mapping microviscosities in live cells with photoswitching kinetics of Dronpa-3 as a contrast mechanism. (*A*) Histograms of the decay rate of Dronpa-3 under 488-nm irradiation at 100 μW in buffers with different percentages of glycerol (0% dark red; 10% red; 20% orange; 40% dark yellow; 60% green; 70% pale blue; 80% blue; and 90% purple). (*B*) Images of Dronpa-3 that are expressed alone in an HEK 293T cell. (*C* and *D*) Images of Dronpa-3 fused with histone H2B protein and expressed in an HEK 293T cell. (*C*) Images were taken while the cell did not undergo mitosis. (*D*) Images were taken while the cell underwent mitosis. In *B*, *C*, and *D*, the fluorescence intensity-based image, the photoswitching rate-based image, and the corresponding decay rate histogram are shown.

mated to be close to 3.0 mPa·s, which is indeed consistent with earlier reports using GFP fluorescence recovery after photobleaching (FRAP) (26). In the case of Dronpa-3 fused with H2B protein, when cells do not undergo mitosis (Fig. 6*C*), the observed decay rate indicates a more viscous chromatin environment experienced by H2B than that of the cytoplasm (slightly higher than that of a 60% glycerol buffer). When cells undergo mitosis (Fig. 6*D*), the observed decay rate exhibits an even more heterogeneous variation of viscosity, possibly due to the densely packed chromosomes, ranging from those of a 0 to 90% glycerol buffer. More images are shown in Fig. S2. Such a remarkable heterogeneity in the distributions of the microviscosity experienced by H2B might be related to the recently observed heterogeneous chromatin compaction detected by fluorescence anisotropy of H2B-EGFP (33).

Conclusion

In summary, we report here on the viscosity sensing property of the photophysics of the photochromic fluorescence protein Dronpa and its mutant. This finding is a special example of fluorescent proteins in which the external environment could exert a mechanical effect on the internal chromophore, making Dronpa an intermediate between the fully exposed organic dyes and the normal FPs whose chromophores are completely shielded. The critical protein conformational flexibility could be responsible not only for the emergence of the photoswitching capability of the Dronpa family, but also for the delicate coupling between the *cis-trans* isomerization of the internal chromophore and the environment outside the protein. This observation is reminiscent of the protein conformational cascade during signal transduction in the rhodopsin family. These insights could shed light on the molecular mechanism of the protein photochromic effect and enhance further protein engineering toward improved photophysical properties.

On the bioimaging side, this genetically encoded viscosity reporter could enable characterization of the crowed microenvironment experienced by any specific proteins of interest via protein fusion, although we only demonstrated H2B in this study. Given the fact that intracellular viscosity and macromolecular crowding play an important role in processes such as signal transduction, nuclear envelope function, chromatin localization, ribonucleoprotein assembly, and diffusion of reactive oxygen species (34–36), this unique reporter could provide valuable mechanistic information about protein function in the crowded and dynamic cellular environment. For example, the observed heterogeneous microviscosity throughout the cell nucleus shown in Fig. 6, together with the reported spatiotemporal heterogeneity of chromatin compaction/fluidity (33), could have broader implications in understanding chromatin condensation and transcription control within live cells.

Materials and Methods

Fluorescence Microscopy. Our experimental setup is a modified confocal microscope equipped with two-color laser excitation (Fig. 2). The 488-nm beam was spatially expanded and collimated before it was collinearly combined with the 405-nm beam that had a smaller beam size. As a result, the focal spot of 488-nm beam in the sample is smaller and completely covered by the 405-nm illumination area. Temporally, samples were continuously illuminated with the 488-nm light, while a 1 ms pulse of 405-nm light was applied

every 30 ms. A fluorescence filter and a 50 μm pinhole were used in front of the photomultiplier tube to reject the fundamental laser light and to ensure confocality. To acquire fluorescence trajectories and images, the sample was moved by a closed-loop piezo stage in a raster scanning pattern. A home-written LabVIEW program was used to control the stage scanning, to synchronize 405-nm pulse firing and to record fluorescence signals via a data acquisition card (Fig. 2, *Lower*). For data analysis, another LabVIEW program was used to extract initial 1.5-ms fluorescence decay trajectories, to fit the extracted traces with single-exponential decay and to form the decay rate-based images.

Plasmid Construction. Dronpa expression vector and Dronpa-3 cloning vector were purchased from MBL International Corporation. The DNA fragment containing the Dronpa gene was amplified by PCR and subcloned into the *NdeI* and *XhoI* site of pAED4 plasmid. The pAED4-Dronpa vector and the pAED4-Dronpa-3 vector were later used to express Dronpa protein in *Escherichia coli* BL21 cells. For in vivo experiments, the H2B-Dronpa-3 plasmids and the Dronpa-3 expression vector were constructed by replacing the EGFP gene in the H2B-GFP plasmid with the Dronpa-3 gene and removing the H2B gene from the H2B-Dronpa-3 plasmids, respectively. Both pAED4 plasmid and H2B-GFP plasmid are generous gifts from Virginia Cornish (Columbia University, New York, NY).

Protein Production, Purification, and Transfection. Dronpa and Dronpa-3 proteins were expressed in *E. coli* BL21 cells and purified by His-tag affinity and subsequent size-exclusion chromatography according to standard procedures. A final protein concentration of $10 \sim 50$ μM was prepared in 50 mM sodium phosphate buffer at pH 8.0 with 300 mM NaCl and 0, 10, 20, 40, 60, 70, 80, or 90% (vol/vol) of glycerol. Homogeneity was confirmed to be more than 99% by SDS-PAGE analysis. The HEK 293T cells were seeded in plates at a density of 2×10^5 cells in 2 mL of DMEM with 10% FBS and 1% penicillin/streptomycin. Dronpa-3 and H2B-Dronpa-3 DNA constructs were transiently transfected into HEK 293T cells using transfection reagent FuGENE HD, separately.

ACKNOWLEDGMENTS. We thank Professors Virginia Cornish, Michael Sheetz, and John Hunt for sharing lab equipment. We thank Chaoran Jing, Chi Wang, and Zhixing Chen for their help on protein expression, purification, and cell culture. W.M. acknowledges start-up funds from Columbia University.

1. Chalfie M, Tu Y, Euskirchen G, Ward WW, Prasher DC (1994) Green fluorescent protein as a marker for gene expression. *Science* 263:802–805.
2. Tsien RY (1998) The green fluorescent protein. *Annu Rev Biochem* 67:509–544.
3. Lippincott-Schwartz J, Patterson GH (2003) Development and use of fluorescent protein markers in living cells. *Science* 300:87–91.
4. Newman RH, Fosbrink MD, Zhang J (2011) Genetically encodable fluorescent biosensors for tracking signaling dynamics in living cells. *Chem Rev* 111:3614–3666.
5. Yang F, Moss LG, Phillips GN (1996) The molecular structure of green fluorescent protein. *Nat Biotechnol* 14:1246–1251.
6. Suhling K, Davis DM, Phillips D (2002) The influence of solvent viscosity on the fluorescence decay and time-resolved anisotropy of green fluorescent protein. *J Fluoresc* 12:91–95.
7. Suhling K, et al. (2002) Imaging the environment of green fluorescent protein. *Biophys J* 83:3589–3595.
8. Borst JW, Hink MA, van Hoek A, Visser AJWG (2005) Effects of refractive index and viscosity on fluorescence and anisotropy decays of enhanced cyan and yellow fluorescent proteins. *J Fluoresc* 15:153–160.
9. Lippincott-Schwartz J, Patterson GH (2008) Fluorescent proteins for photoactivation experiments. *Methods Cell Biol* 85:45–61.
10. Lukyanov KA, Chudakov DM, Lukyanov S, Verkhusha VV (2005) Photoactivatable fluorescent proteins. *Nat Rev Mol Cell Biol* 6:885–891.
11. Mizuno H, et al. (2003) Photo-induced peptide cleavage in the green-to-red conversion of a fluorescent protein. *Mol Cell* 12:1051–1058.
12. Chudakov DM, et al. (2003) Kindling fluorescent proteins for precise in vivo photolabeling. *Nat Biotechnol* 21:191–194.
13. Ando R, Mizuno H, Miyawaki A (2004) Regulated fast nucleocytoplasmic shuttling observed by reversible protein highlighting. *Science* 306:1370–1373.
14. Andresen M, et al. (2005) Structure and mechanism of the reversible photoswitch of a fluorescent protein. *Proc Natl Acad Sci USA* 102:13070–13074.
15. Stiel AC, et al. (2008) Generation of monomeric reversibly switchable red fluorescent proteins for far-field fluorescence nanoscopy. *Biophys J* 95:2989–2997.
16. Wilmann PG, et al. (2006) The 1.7 Å crystal structure of Dronpa: A photoswitchable green fluorescent protein. *J Mol Biol* 364:213–224.
17. Andresen M, et al. (2007) Structural basis for reversible photoswitching in Dronpa. *Proc Natl Acad Sci USA* 104:13005–13009.
18. Stiel AC, et al. (2007) 1.8 Å bright-state structure of the reversibly switchable fluorescent protein Dronpa guides the generation of fast switching variants. *Biochem J* 402:35–42.
19. Mizuno H, et al. (2008) Light-dependent regulation of structural flexibility in a photochromic fluorescent protein. *Proc Natl Acad Sci USA* 105:9227–9232.
20. Ando R, Flors C, Mizuno H, Hofkens J, Miyawaki A (2007) Highlighted generation of fluorescence signals using simultaneous two-color irradiation on Dronpa mutants. *Biophys J* 92:L97–L99.
21. Flors C, et al. (2007) A stroboscopic approach for fast photoactivation-localization microscopy with Dronpa mutants. *J Am Chem Soc* 129:13970–13977.
22. Andresen M, et al. (2008) Photoswitchable fluorescent proteins enable monochromatic multilabel imaging and dual color fluorescence nanoscopy. *Nat Biotechnol* 26:1035–1040.
23. Kwon OY, Kwon IC, Song HK, Jeon H (2008) Real-time imaging of NF-AT nucleocytoplasmic shuttling with a photoswitchable fluorescence protein in live cells. *Biochim Biophys Acta* 1780:1403–1407.
24. Shroff H, et al. (2007) Dual-color superresolution imaging of genetically expressed probes within individual adhesion complexes. *Proc Natl Acad Sci USA* 104:20308–20313.
25. Mizuno H, et al. (2010) Higher resolution in localization microscopy by slower switching of a photochromic protein. *Photochem Photobiol Sci* 9:239–248.
26. Swaminathan R, Hoang CP, Verkman AS (1997) Photobleaching recovery and anisotropy decay of green fluorescent protein GFP-S65T in solution and cells: Cytoplasmic viscosity probed by green fluorescent protein translational and rotational diffusion. *Biophys J* 72:1900–1907.
27. Habuchi S, et al. (2005) Reversible single-molecule photoswitching in the GFP-like fluorescent protein Dronpa. *Proc Natl Acad Sci USA* 102:9511–9516.
28. Li X, Chung LW, Mizuno H, Miyawaki A, Morokuma K (2010) Primary events of photodynamics in reversible photoswitching fluorescent protein Dronpa. *J Phys Chem Lett* 1:3328–3333.
29. Pernodet N, Maaloum M, Tinland B (1997) Pore size of agarose gels by atomic force microscopy. *Electrophoresis* 18:55–58.
30. Cotlet M, et al. (2001) Excited-state dynamics in the enhanced green fluorescent protein mutant probed by picosecond time-resolved single photon counting spectroscopy. *J Phys Chem B* 105:4999–5006.
31. Jung G, Wiehler J, Zumbusch A (2005) The photophysics of green fluorescent protein: Influence of the key amino acids at positions 65, 203, and 222. *Biophys J* 88:1932–1947.
32. van Manen H-J, et al. (2008) Refractive index sensing of green fluorescent proteins in living cells using fluorescence lifetime imaging microscopy. *Biophys J* 94:L67–L69.
33. Banerjee B, Bhattacharya D, Shivashankar GV (2006) Chromatin structure exhibits spatio-temporal heterogeneity within the cell nucleus. *Biophys J* 91:2297–2303.
34. Lang I, Scholz M, Peters R (1986) Molecular mobility and nucleocytoplasmic flux in hepatoma cells. *J Cell Biol* 102:1183–1190.
35. Marshall WF, et al. (1997) Interphase chromosomes undergo constrained diffusional motion in living cells. *Curr Biol* 7:930–939.
36. Kues T, Dickmanns A, Lührmann R, Peters R, Kubitscheck U (2001) High intranuclear mobility and dynamic clustering of the splicing factor U1 snRNP observed by single particle tracking. *Proc Natl Acad Sci USA* 98:12021–12026.

Supporting Information

Kao et al. 10.1073/pnas.1115311109

SI Materials and Methods

Fluorescence Microscopy. Our experimental setup is shown in Fig. 2. A 405-nm diode laser (Cube 405-50C, Coherent) and a 488-nm Sapphire laser (Sapphire 488-50, Coherent) are used as the excitation source on a home-built confocal microscope. The 488-nm beam is spatially expanded and collimated before it is collinearly combined with the 405-nm beam, which has a smaller beam size by a dichroic mirror (LM-01-427-25, Semrock). Both beams are sent into an inverted microscope (IX71, Olympus). A laser dichroic mirror (FF495-Di03-25 × 36, Semrock) reflects the excitation light into an oil immersion objective lens (UPlanSApo, 100×, 1.4 N.A., Olympus). The objective lens focuses the 488-nm laser beam into a diffraction-limited spot. In contrast, the 405-nm laser beam has a smaller beam size before entering the microscope and underfills the back aperture of the objective. As a result, the focal spot of 488-nm beam in the sample is smaller and completely covered by the 405-nm illumination area. The same objective collects the epifluorescence signal, which is then directed to the microscope's primary image plane. A fluorescence filter (BLP01-488R, Semrock) was used in front of the photomultiplier tube (PMT) (R9110, Hamamatsu) to reject the fundamental laser light. A 50-μm pinhole in front of the PMT ensures confocality.

The PMT is equipped with a wide-bandwidth amplifier module (10 MHz; M7279, Hamamatsu) and the PMT current output is further amplified by a low-noise current preamplifier (SR570, Stanford Research Systems). To acquire fluorescence trajectories and images, the sample is moved by a closed-loop piezo stage (P-545.2R7, Physik Instrumente) in a raster scanning pattern. A home-written LabVIEW program is used to control the stage scanning, to synchronize 405-nm pulse firing, and to record fluorescence signals via a data acquisition card (PCI-6259, National Instruments). The synchronization between the stage step-scanning and the 405-nm pulse firing is shown in Fig. 2, *Lower*. For data analysis, another home-written LabVIEW program is used to extract initial 1.5-ms fluorescence decay trajectories and to fit the extracted traces with single-exponential decay for those in vitro and in vivo experiments and to form images for those in vivo experiments.

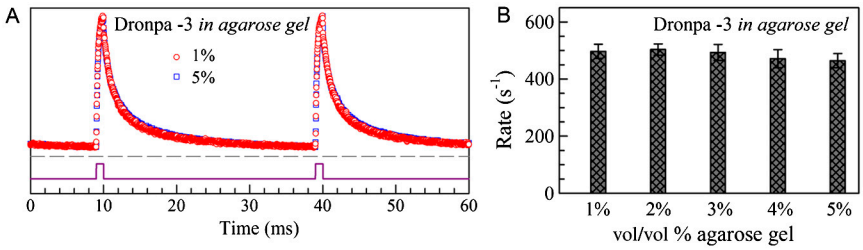

Fig. S1. Fluorescence time course and decay rates of Dronpa-3 in agarose gels of different percentages. (*A*) Fluorescence time courses of Dronpa-3 in agarose gels of 1 and 5% concentrations under the corresponding on-off illumination scheme of 405-nm light (488-nm light is continuously on). The gray dashed line indicates the fluorescence background level. (*B*) The decay rate Dronpa-3 in agarose gel of five different percentages. No clear difference of the decay rates was observed.

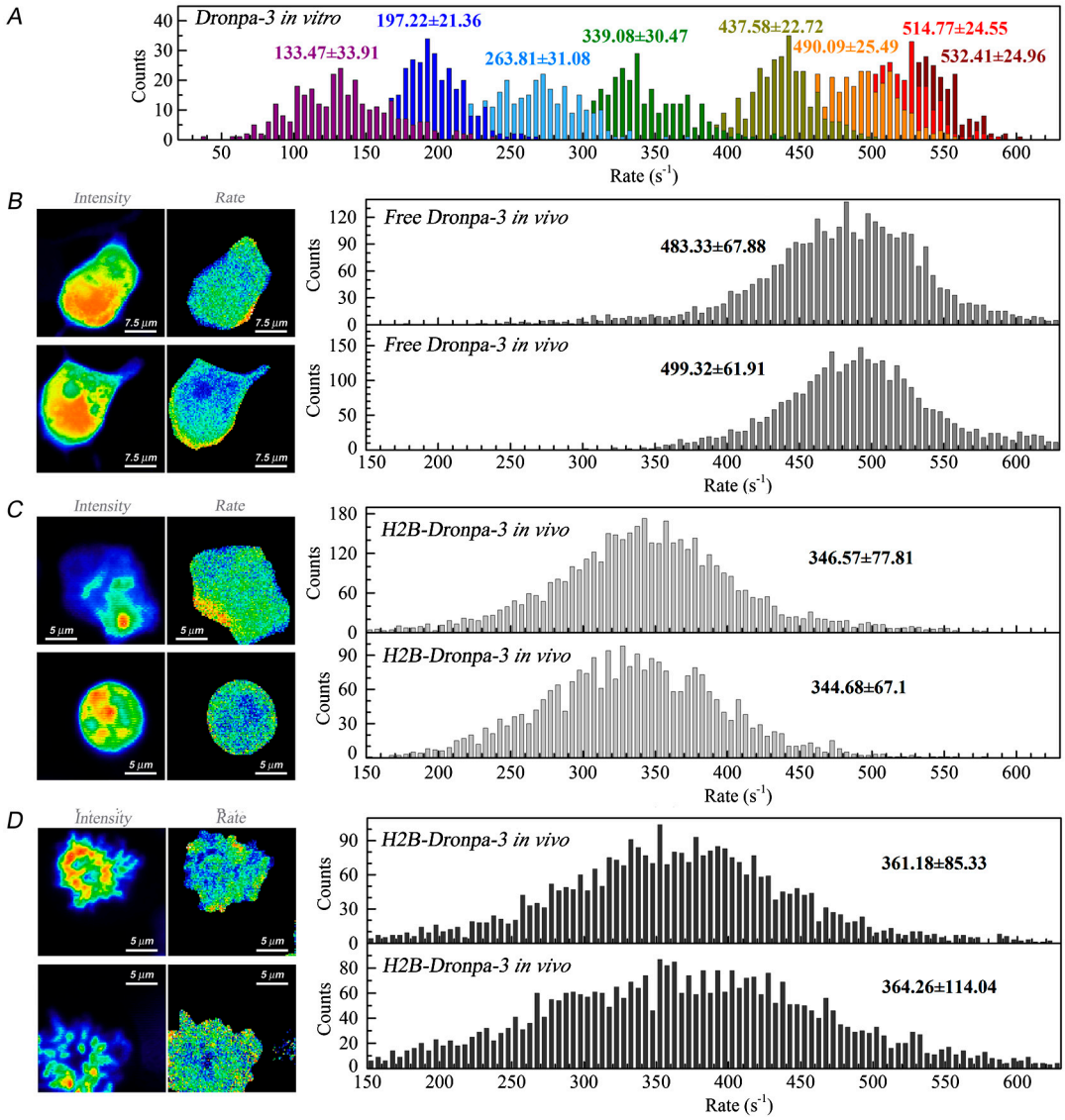

Fig. S2. Mapping microviscosities in live cells with photoswitching kinetics of Dronpa-3 as a contrast mechanism. (*A*) Histograms of the decay rate of Dronpa-3 under 488-nm irradiation at 100 μW in buffers with different percentages of glycerol (0% dark red; 10% red; 20% orange; 40% dark yellow; 60% green; 70% pale blue; 80% blue; and 90% purple). (*B*) Images of Dronpa-3 that are expressed alone in an HEK 293T cell. (*C* and *D*) Images of Dronpa-3 fused with histone H2B protein and expressed in an HEK 293T cell. (*C*) Images were taken while the cell did not undergo mitosis. (*D*) Images were taken while the cell underwent mitosis. In *B*, *C*, and *D*, the fluorescence intensity-based image, the photoswitching rate-based image, and the corresponding decay rate histogram are shown.

Table S1. The fluorescence decay rates of Dronpa in buffer with various percentages of glycerol

	488-nm laser power			
Dronpa (% glycerol)	100 μW	200 μW	400 μW	1,000 μW
0[a]	152.81	197.61	229.85	282.28
10	144.74	188.85	218.94	271.89
20	135.17	178.75	199.28	252.52
40	126.85	160.91	183.45	215.37
60	116.00	140.12	170.43	193.64
70	106.62	123.45	144.64	169.84
80	103.53	112.38	135.30	159.32
90[b]	97.71	103.38	112.15	118.87
Ratio[a]/[b]	1.56	1.91	2.04	2.37

All rates are in the unit of second^{-1}. Ratio is obtained by dividing [a] by [b].

Table S2. The fluorescence decay rates of Dronpa-3 in buffer with various percentages of glycerol

	488-nm laser power			
Dronpa-3 (% glycerol)	100 μW	200 μW	400 μW	1,000 μW
0[a]	532.41	656.14	741.52	834.32
10	514.77	625.52	699.73	784.22
20	490.09	589.41	665.79	735.41
40	437.58	521.04	573.09	654.89
60	339.08	427.38	492.70	576.18
70	263.81	357.95	426.45	482.84
80	197.22	285.74	338.43	380.70
90[b]	133.47	167.24	193.67	223.98
Ratio[a]/[b]	3.99	3.92	3.83	3.72

All rates are in the unit of second^{-1}. Ratio is obtained by dividing [a] by [b].